Electronic Supplementary Material (ESI) for Soft Matter.

Structural characterization of fibrous synthetic hydrogels using fluorescence microscopy

Johannes Vandaele,[1] Boris Louis,[1,2] Kaizheng Liu,[3] Paul H.J. Kouwer,[3] Rafael Camacho,[1] Susana Rocha,*[1]

[1] Molecular Imaging and Photonics, KU Leuven, 3001 Leuven, Belgium
[2] Division of Chemical Physics and NanoLund, Lund University, 22100 Lund, Sweden
[3] Institute for Molecules and Materials, Radboud University, 6525 AJ Nijmegen, The Netherlands

Supporting Table S1. Pore network properties of the different hydrogels.

Hydrogel	Porosity (%)	Connectivity		Throat Diameter (µm)		Pore Diameter (µm)	
	Mean ± Std	Median	Mean ± Std	Median	Mean ± Std	Median	Mean ± Std
S1	39 ± 3	3	3.2 ± 2.5	1.1	1.0 ± 0.6	1.8	1.9 ± 0.6
L1	41 ± 6	3	3.7 ± 2.5	1.1	1.0 ± 0.5	1.8	1.8 ± 0.5
S05	53 ± 3	5	5.2 ± 3.4	1.1	1.3 ± 0.8	2.3	2.5 ± 0.9
L05	56 ± 4	5	5.8 ± 3.1	1.3	1.4 ± 0.7	2.5	2.6 ± 0.8
S025	68 ± 5	5	6.0 ± 4.2	1.3	1.5 ± 1.1	3.3	3.7 ± 1.8
L025	68 ± 4	5	6.1 ± 3.6	1.6	1.9 ± 1.2	3.5	3.7 ± 1.6

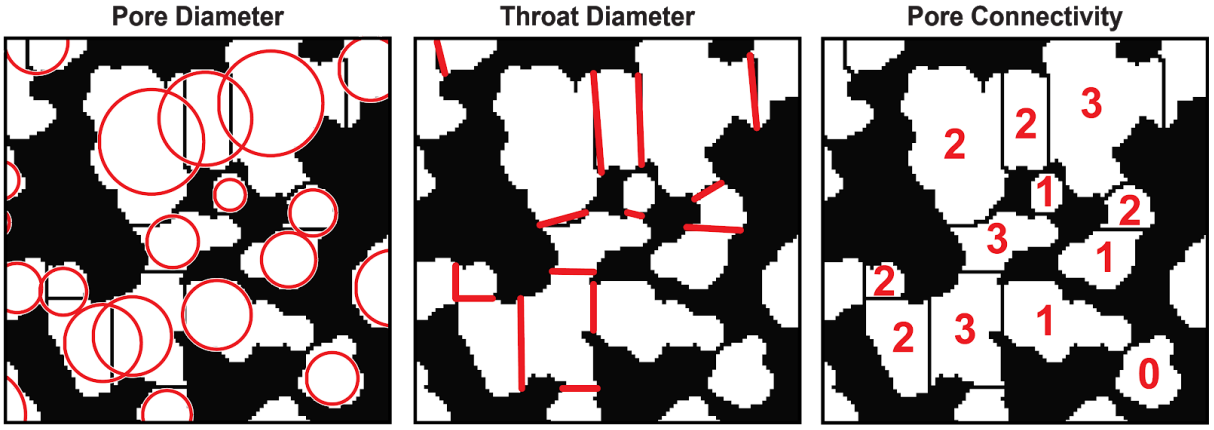

Supporting Figure S1. Determination of network properties. From the watershed segmented images (Figure 2d), several parameters are calculated for each area. **(a)** The pore diameter is defined as the double of the largest distance within the region (determined in the distance map). **(b)** The throat diameter is defined as the length of the line separating two regions. **(c)** The connectivity is calculated by counting the number of adjacent regions.

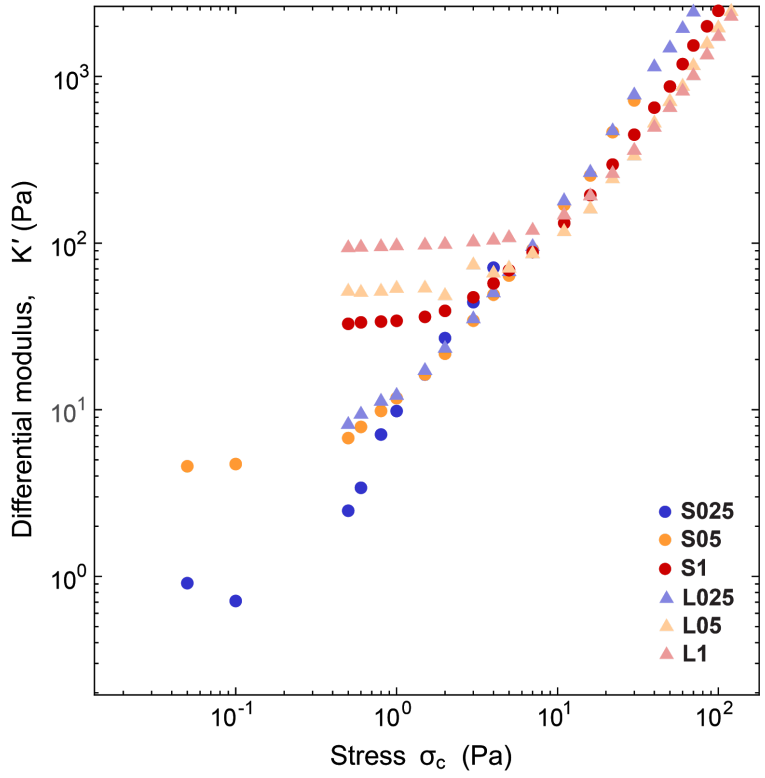

Supporting Figure S2. Mechanical properties of PIC gels used in this work. Differential modulus K′ as a function of applied stress (T = 37 °C) for gels P1−P6. The plateau values at low stress correspond to the modulus in the linear viscoelastic regime. Circles: short polymer, triangles: long polymer.

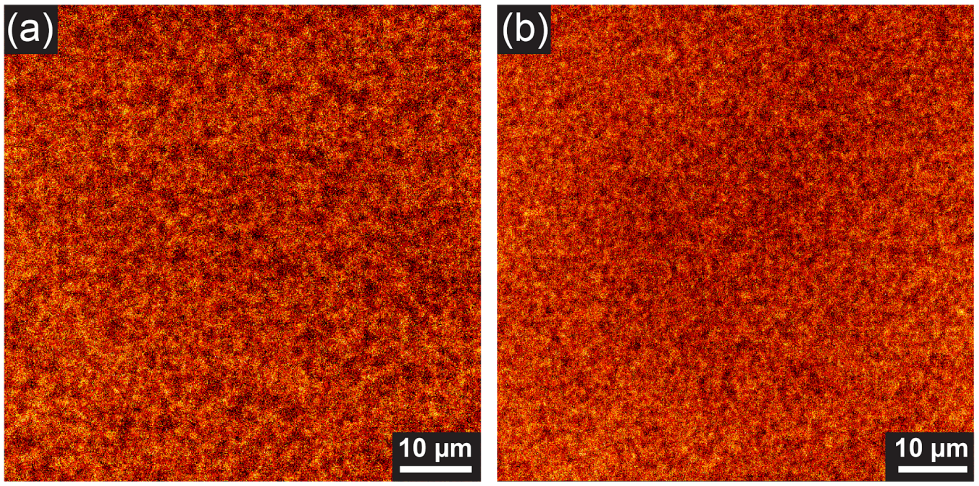

Supporting Figure S3. Hydrogel network at higher concentrations. Representative fluorescence images of hydrogels prepared with short (a) and long (b) PIC polymers, labelled with TAMRA, using a concentration of 2 mg/mL.

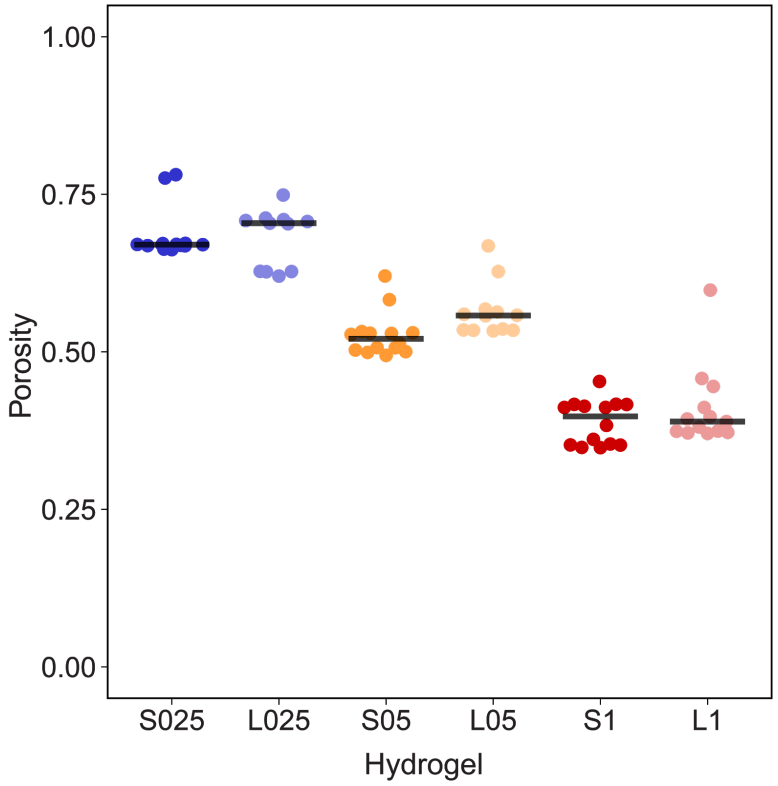

Supporting Figure S4. Porosity of the hydrogels used. The degree of porosity was calculated using the segmented images (Figure 1c). For each volume imaged, a mean value was calculated.

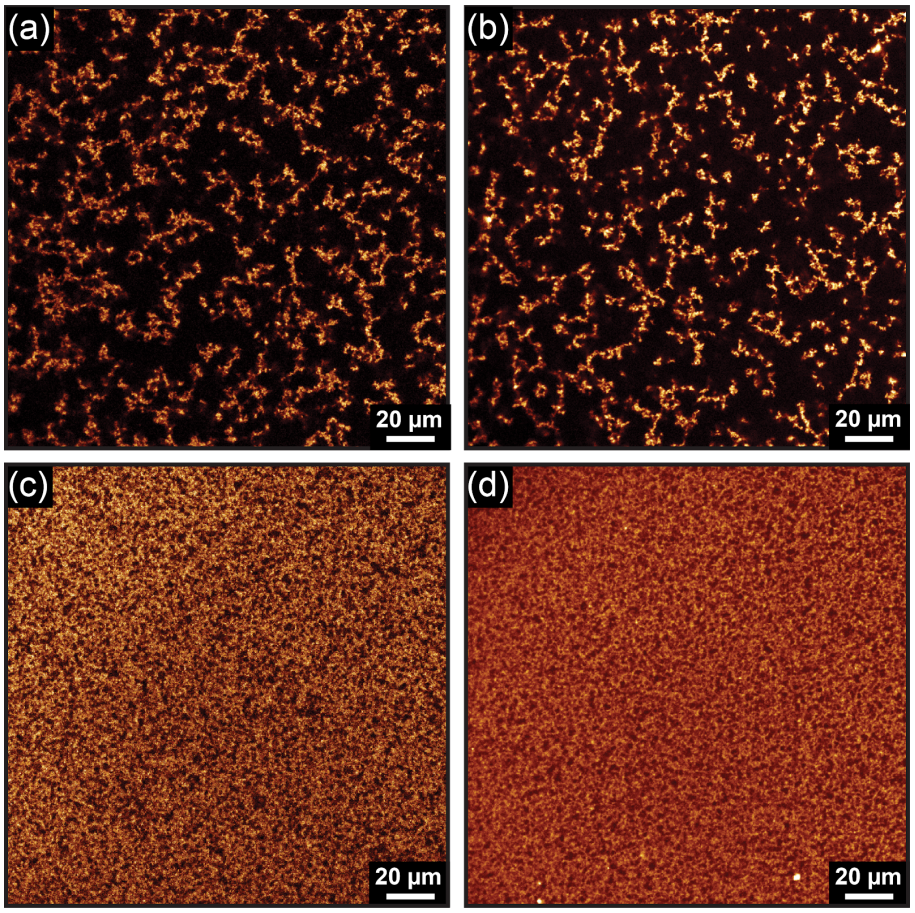

Supporting Figure S5. Representative fluorescence images of other hydrogels used. **(a)** S025 **(b)** L025 **(c)** S1 **(d)** L1. The polymer length does not affect the fiber architecture significantly.

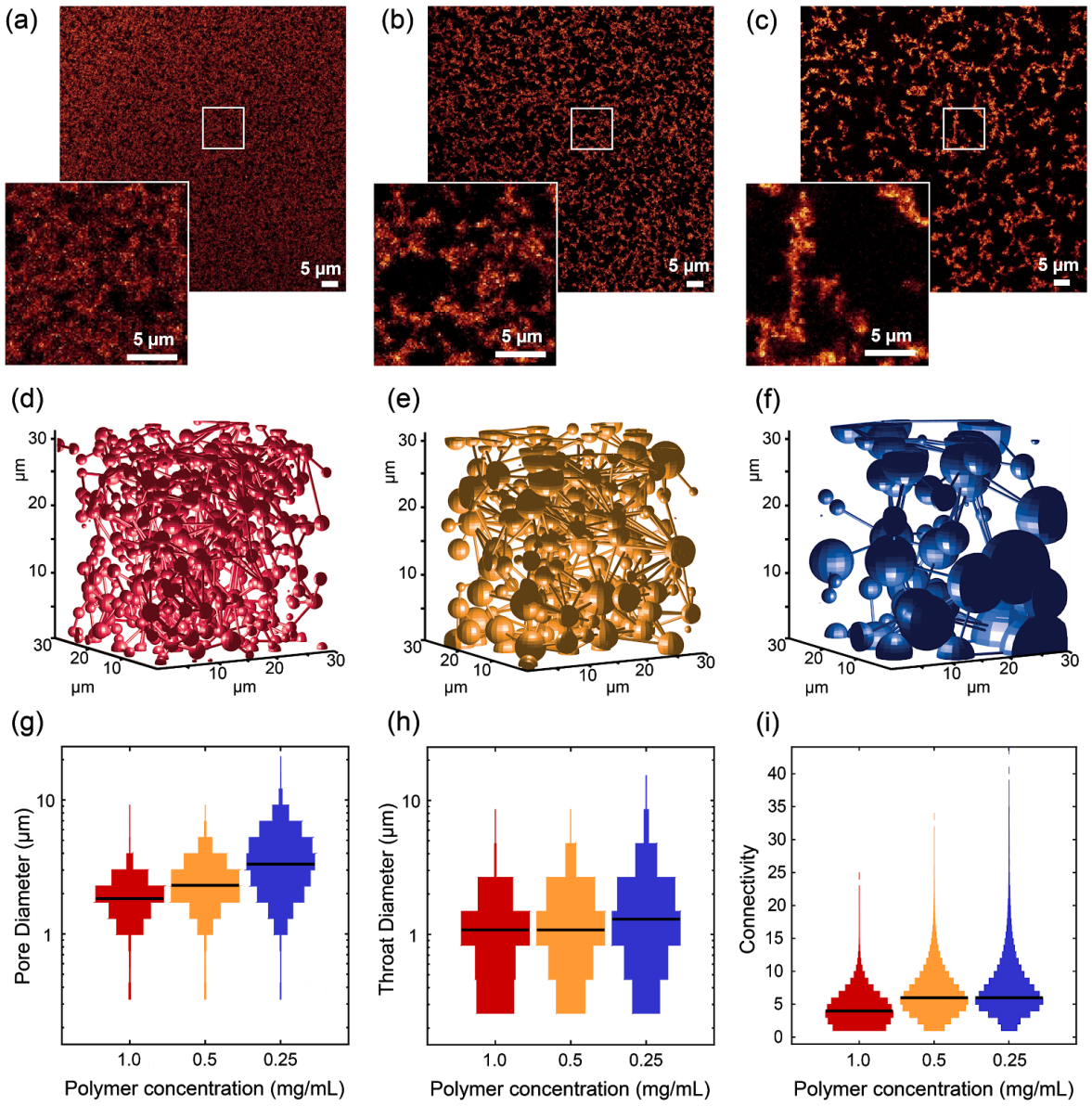

Supporting Figure S6: Influence of polymer concentration on fiber architecture of gels prepared from short polymers. (a-c) Representative fluorescence images of labelled short PIC polymers at the concentrations of 1 mg/mL, S1 (a), 0.5 mg/mL, S05 (b) and 0.25 mg/mL, S025 (c). The insets on the lower left corner are magnified images of the region indicated by the white square. **(d-f)** Schematic representation of the pore diameter (spheres) and connectivity (sticks) in 3D of S1 (d), S05 (e) and S025 (f). **(g)** Distribution of the pore diameter of the different hydrogels. **(h)** Distribution of the throat diameter of the different hydrogels. **(i)** Distribution of the pore connectivity in different hydrogels. The black lines indicate the median values of the distribution.

Supporting Note 1 - image analysis

1) Sensitivity

Our segmentation method chose a threshold locally based on first order statistics (mean of the area) and the sensitivity. A higher sensitivity will mean that more pixels will be assessed as foreground (polymer). Therefore, a low sensitivity will tend to assess too few pixels as foreground while a too high sensitivity will tend to assess too many pixels as foreground.

Intuitively, the midrange of sensitivity should be used in most cases (0.4 - 0.6). Choosing the sensitivity is typically performed by comparing the segmented images to the original image for different thresholds and evaluating by eye which one seems to be the best. As shown in Fig. Sxx we can see that the sensitivity of 0.2 is better for 0.25 mg/mL while the sensitivity of 0.6 is better for 0.5 mg/mL. A drawback of this approach is that it remains quite subjective and is definitely not quantitative. Therefore, it is challenging to determine which sensitivity threshold will yield the best segmentation.

Typically, scientists using segmentation have solved this problem by performing a segmentation by hand by "an expert" (in the type of features processed) to which the automated software is compared to. Therefore, we segmented by hand the network for two different concentrations of the network (0.25 mg/mL and 0.50 mg/mL). We segmented 250 pixel x 250 pixel x 17 z slices for 0.25 mg/mL and 250 x 250 x 11 for 0.50 mg/mL. Our software was run on the same dataset using adaptive and global thresholding. For the adaptive threshold, we investigate the influence of the sensitivity by analyzing the data with different sensitivity values (0.2, 0.4, 0.6 and 0.8).We looked at 3 different metrics (precision, recall and the bf score)[1] to compare with the hand segmentation. The results are shown in Fig. S7.

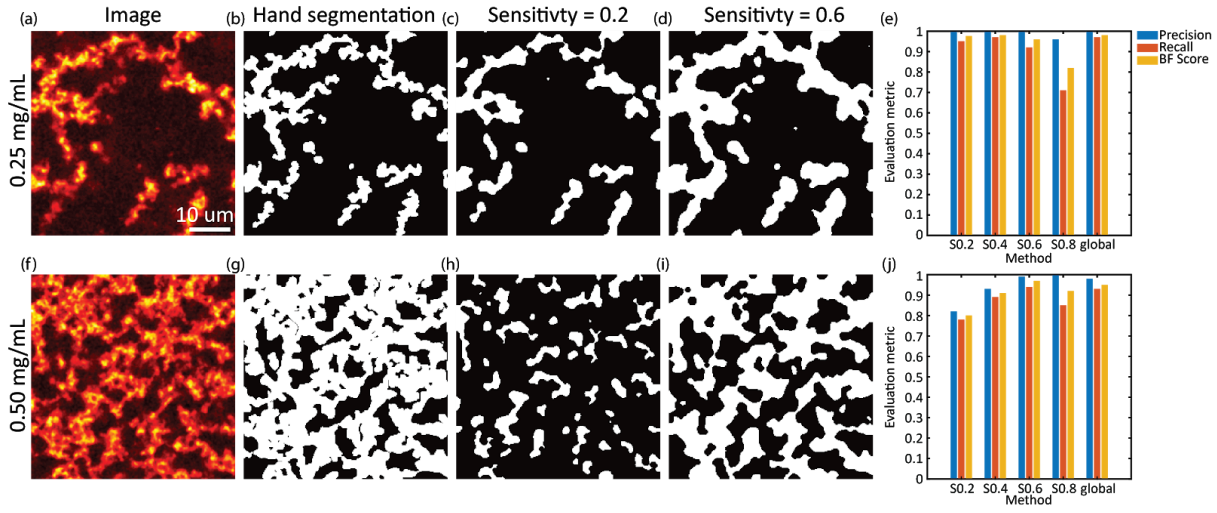

Supporting Figure S7: Comparison of different segmentation sensitivity. (a) 50 x 50 µm image of PIC network with a polymer concentration of 0.25 mg/ml **(b)** A manually segmented image of image (a) **(c)** Result of the adaptive threshold with a sensitivity of 0.2 **(d)** Result of the adaptive threshold with a sensitivity of 0.6 **(e)** Precision, recall and bf score for different segmentation methods compared to hand segmentation. **(f)** 50 x 50 µm image of PIC network with a polymer concentration of 0.5 mg/ml **(g)** A manually segmented image of image (f) **(h)** Result of the adaptive threshold with a sensitivity of 0.2) **(i)** Result of the adaptive threshold with a sensitivity of 0.6). **(j)** Precision, recall and bfscore for different segmentation methods compared to hand segmentation.

The precision is calculated based on the number of true positives in the automated segmentation compared to the hand segmentation. It is a useful metric but easily misleading because a single white pixel in the foreground region would yield 100 % precision. Therefore, we also use recall which considers both false negative and the bf score (which takes precision and recall) together in one metric.

$$Precision = \frac{tp}{(tp+fp)}$$

$$Recall = \frac{tp}{(tp+fp)}$$

$$Bfscore = \frac{(2*Precision*Recall)}{(Precision+Recall)}$$

Our results show that at low concentration of the polymer, most of the sensitivity values perform well with precision recall and bfscore >90% except for 0.8 sensitivity. The 0.4 sensitivity is the one performing best together with global thresholding. However, for 0.5 mg/mL the lowest sensitivity is failing severely as can be seen from both the segmented image and the scores. A sensitivity of 0.6 is performing the best together with global thresholding.

Willing to use a single sensitivity across the acquired dataset, we decided to keep 0.6 as it seems to perform well on both low and high concentrations. We decided to use the adaptive threshold because some images in our dataset presented a non-homogeneous background, which made global thresholding worse in these cases. If the reader or potential users of our code doesn't need the flexibility of a threshold and possesses a dataset with a homogeneous background, we would however advise to use the global thresholding also available in the package as it seems to be quite robust.

2) Pore-size analysis comparison

We compared our algorithm with the simplified bubble analysis[2–4]. The main reason for this choice is that the bubble analysis is quite renowned in the field and the paper concerning the simplified version provided the matlab code allowing us to compare directly the two methods in a straightforward manner.

In order to compare the two algorithms we run both algorithms in 2D on several slices for each concentration studied (0.25 mg/mL, 0.5 mg/mL and 1 mg/mL). We then plotted the pores found by the two algorithms on top of the segmented image for visual comparison and plot the histogram of the sizes for more quantitative comparison. The results are shown in Fig. S8.

Visually, one difference is striking: the number of "pores" detected is much higher for the simplified bubble analysis. Basically in that analysis, anything is considered as pore and so even "tubes" connecting different pores. This is a drawback that was also pointed out in a response to the paper presenting this method which suggested a post processing step to improve the results. Our code already contains the necessary post-processing steps. A direct consequence of the higher number of pores and the detection of tubes is that the distribution of pore-sizes is wrongly shifted toward smaller pores compared to our algorithm. This difference is more pronounced for more porous networks as shown in Fig.S8. Although this comparison is performed in 2D as it is easier to visualize, it is clear that the effect will be even more pronounced when shifting to 3D.

Furthermore, while using conventional bubble analysis only the distribution of the pore diameter is calculated, using our analysis, each pore is post processed to obtain several properties. Here is a list of these parameters and their definition:

1) Diameter: displayed on the left panel of Supporting Figure S7 as red circles. It represents the biggest circle that can be fit into the pore but does not use the separation performed by the watershed, only the local maxima. Therefore, it is the closest to the conventional method and describes quite correctly the size of object that could navigate through the pores.
2) Throat: the diameter of the "connection" between pores. Together with the diameter it fully describes the pores obtained within the watershed. The description by only the diameter could feel undersampled compared to the reality but by combining with the throat it provides the full description of the pores. The throat cannot be calculated with the conventional method but is somewhat included in the oversampling although one cannot disentangle the real pores from the throat and the oversampled pores.
3) Connectivity: This parameter describes which pore is connected to other pore(s), giving an idea of the interconnectivity of the pores. This cannot be calculated by the conventional method and is a really important parameter for the understanding of the network.
4) Volume: Volume of the pores as given after the separation. Despite being an "exact" description of the pores, it carries relatively low information or meaning as the shape of each pore is quite random.

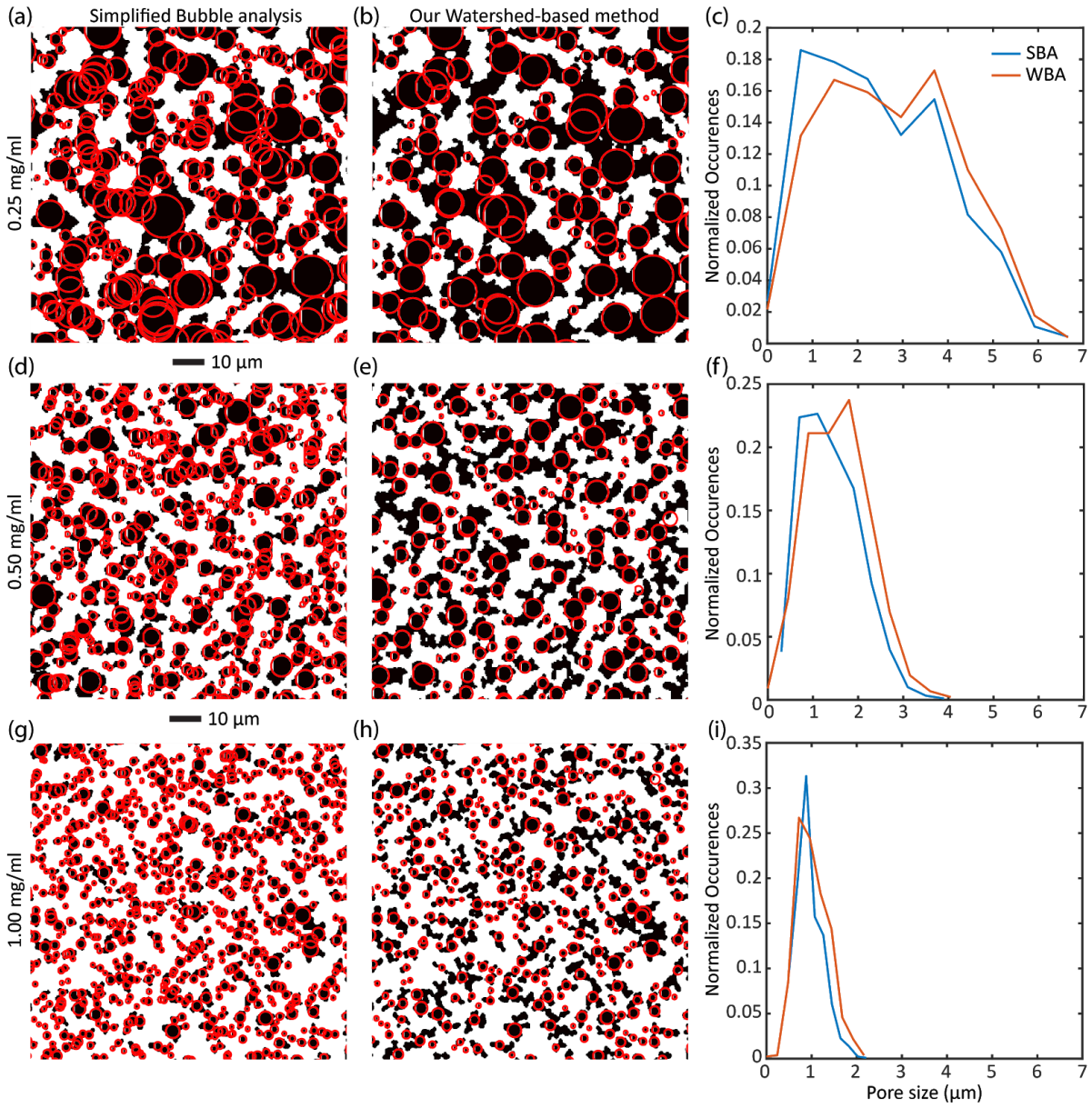

Supporting Figure S8: Pore-size analysis algorithm comparison. (a,d,g) Results of the bubble analysis overlaid on the segmentation image for 0.25, 0.5 and 1 mg/mL respectively. **(b,e,h)** Results of our watershed based analysis overlaid on the segmentation image for 0.25, 0.5 and 1 mg/mL respectively. **(c,f,j)** Distribution of pore size obtained for the two analysis methods for different concentrations. SBA stands for Simplified Bubble Analysis while WBA stands for Watershed-Based Analysis.

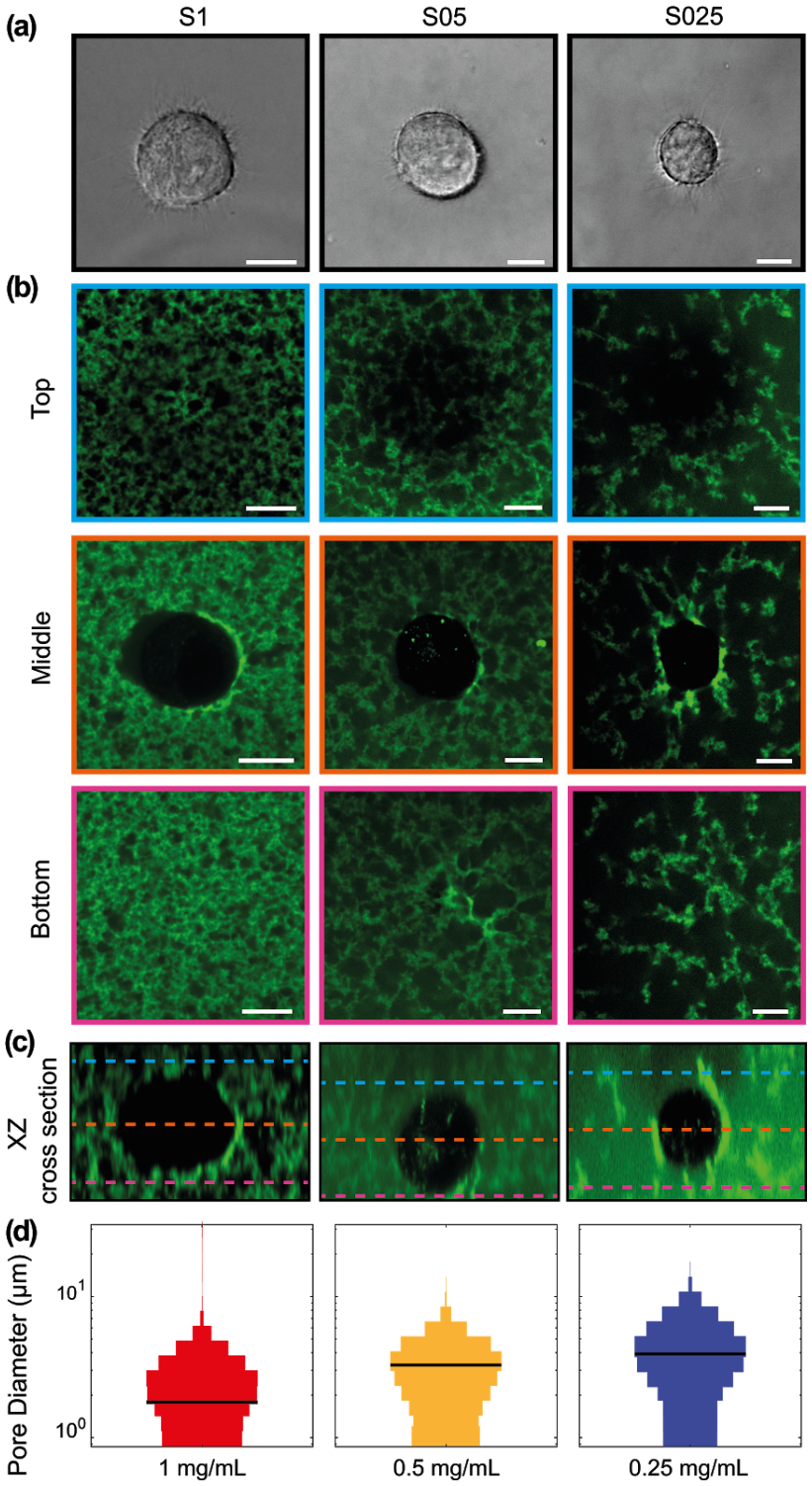

Supporting Figure S9: Influence of cell encapsulation in the network architecture. (a) Representative bright images of HeLa cells after 24h encapsulated in short PIC polymer hydrogels with different concentrations (1 mg/ml, 0,5 mg/ml and 0,25 mg/ml for S1, S05 and S025, respectively). **(b)** Fluorescence images of XY planes acquired below, at the middle of the cell and above the cell **(c)** Fluorescence images of the XZ cross section. The colored dashed lines correspond to the XY planes shown in panel (b). **(d)** Distribution of the pore diameter of the hydrogel in the different samples. The black line indicates the median value of the pore diameter (1.55, 2.0 and 2.9 µm, for 1.0 mg/mL, 0.5 mg/mL and 0.25 mg/mL, respectively). Scale bar: 10 µm.

References

(1) Csurka, G.; Larlus, D.; Perronnin, F. What Is a Good Evaluation Measure for Semantic Segmentation? In *Procedings of the British Machine Vision Conference 2013*; British Machine Vision Association: Bristol, 2013; pp 32.1-32.11. https://doi.org/10.5244/C.27.32.

(2) Molteni, M.; Magatti, D.; Cardinali, B.; Rocco, M.; Ferri, F. Fast Two-Dimensional Bubble Analysis of Biopolymer Filamentous Networks Pore Size from Confocal Microscopy Thin Data Stacks. *Biophys. J.* **2013**, *104* (5), 1160–1169. https://doi.org/10.1016/j.bpj.2013.01.016.

(3) Münster, S.; Fabry, B. A Simplified Implementation of the Bubble Analysis of Biopolymer Network Pores. *Biophys. J.* **2013**, *104* (12), 2774–2775. https://doi.org/10.1016/j.bpj.2013.05.016.

(4) Molteni, M.; Magatti, D.; Cardinali, B.; Rocco, M.; Ferri, F. Response to “A Simplified Implementation of the Bubble Analysis of Biopolymer Networks Pores.” *Biophys. J.* **2013**, *104* (12), 2776–2777. https://doi.org/10.1016/j.bpj.2013.05.015.